ACS OMEGA

Open Access

http://pubs.acs.org/journal/acsodf

Article

Green Synthesis of ZnO and Black TiO_2 Materials and Their Application in Photodegradation of Organic Pollutants

Rab Nawaz,* Habib Ullah, Abdulnoor Ali Jazem Ghanim, Muhammad Irfan, Muzammil Anjum, Saifur Rahman, Shafi Ullah, Zaher Abdel Baki, and Vipin Kumar Oad

Cite This: *ACS Omega* 2023, 8, 36076−36087

Read Online

ACCESS | Metrics & More | Article Recommendations

ABSTRACT: ZnO and black TiO_2 have been selected as the most efficient materials for organic pollution abatement due to their increased efficiency when compared to other materials. However, the concept of green chemistry makes it desirable to design green synthesis approaches for their production. In this study, black TiO_2 was synthesized using an environmentally safe synthetic technique with glycerol as a reductant. ZnO was prepared by using ionic-liquid-based microwave-assisted extracts of *Polygonum minus*. To investigate the materials' potential to photodegrade organic pollutants, methylene blue (MB) and phenol were chosen as model organic pollutants. Both materials were found to exhibit spherical morphologies and a mesoporous structure and were efficient absorbers of visible light. ZnO exhibited electron−hole pair recombination lower than that of black TiO_2. Black TiO_2 was discovered to be an anatase phase, whereas ZnO was found to have a hexagonal wurtzite structure. In contrast to black TiO_2, which had a surface area of 239.99 m^2/g and a particle size of 28 nm, ZnO had a surface area of 353.11 m^2/g and a particle size of 32 nm. With a degradation time of 60 min, ZnO was able to eliminate 97.50% of the 40 mg/L MB. Black TiO_2, on the other hand, could reduce 90.0% of the same amount of MB in 60 min. When tested for phenol degradation, ZnO and black TiO_2 activities were reduced by nearly 15 and 25%, respectively. A detailed examination of both ZnO and black TiO_2 materials revealed that ZnO has more potential and versatility for the degradation of organic pollutants under visible light irradiation.

INTRODUCTION

Heterogeneous photocatalysis is considered a green and environmentally friendly technology for organic pollution reduction. It has two key benefits. First, it may use renewable and sustainable solar energy sources to power photoreactions, making it a promising, green, and economically feasible approach. Second, since its only by-products are water and carbon dioxide, it does not cause any secondary pollution.[1−3] The type of photocatalyst, however, largely determines how well photocatalysis functions to degrade organic pollutants. ZnO and TiO_2 have drawn the most attention among photocatalysts and are thought to be the most effective. Due to their relatively better results in terms of degradation of various organic pollutants, both ZnO and TiO_2 have been suggested for use in environmental applications.[4−8]

TiO_2 is chemically and thermally stable and environmentally biocompatible. However, it responds poorly to solar light. Additionally, it becomes dysfunctional due to the rapid recombination of excited charges on its surface or in the bulk.[9] While ZnO exhibits behavior that is identical to that of TiO_2, it has relatively higher electron mobility. However, it also does not perform flawlessly under visible light. To improve visible light-driven performance for organic pollution reduction various strategies have been adopted.[10] For instance, using a composite of ZnO and TiO_2, Rusman et al.[11] reported 98.26% Congo red dye degradation in just 10 min. Although the composite had a higher efficiency and was prepared from green precursors, *Calopogonium mucunoides* leaf extract, the synthesis process is regarded as being energy intensive because it requires calcining the samples at 800 °C for 2 h.

In a different study, it was discovered that silver-doped ZnO outperformed silver(Ag)-doped TiO_2, as evidenced by the fact that levofloxacin was degraded by 99% by ZnO in 180 min as opposed to 91% by Ag/TiO_2 under ultraviolet light in the same time frame.[9] Under visible light, however, neither type of material performed well because the degradation rates of Ag/ZnO and Ag/TiO_2 were only 56 and 49%, respectively. To enhance its performance in the visible light range, TiO_2 was also doped with other metals. For instance, Ag/TiO_2 was able to remove only 16% of chemical oxygen demand (COD) under visible light when used to degrade organics from actual wastewater, but it could remove 25% of COD under ultraviolet light.[12] Because Pt/TiO_2 could only remove 11% of COD under visible light, doping TiO_2 with platinum (Pt) did not result in any discernible differences.[13] Preparing nanocomposite with reduced graphene oxide was also used to enhance the functionality of ZnO.[14] For instance, the sol−gel method was used to modify ZnO with neodymium(III) oxide (Nd_2O_3) in the presence of a copolymer (Pluronic F-108).[15]

Received: June 14, 2023
Accepted: September 12, 2023
Published: September 22, 2023

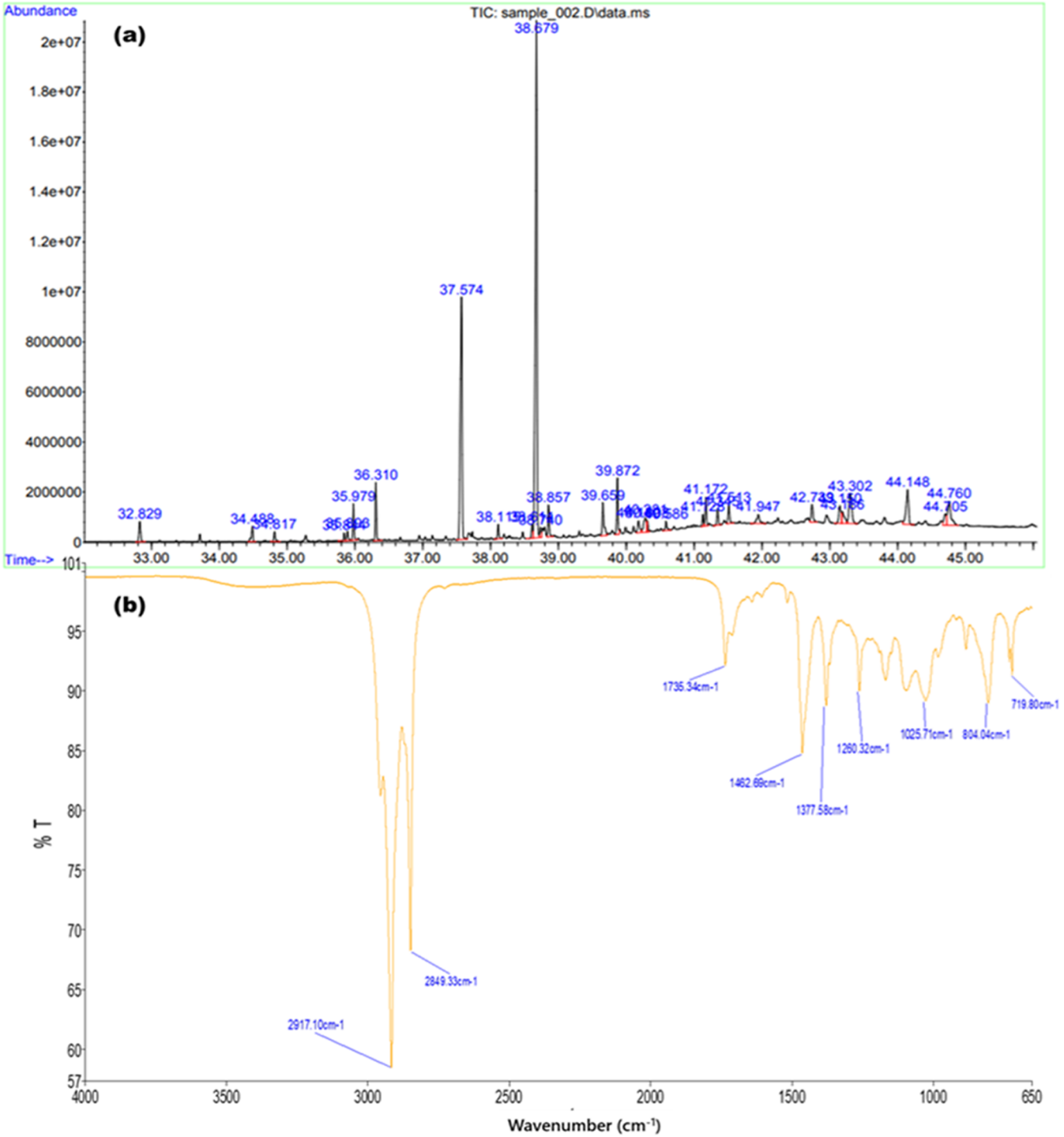

Figure 1. (a) GCMS chromatogram and (b) FTIR spectrum of the plant extract.

According to the study, (Nd_2O_3) modified ZnO degrades tetracycline 8.8 and 163 times more quickly than ZnO and TiO_2, respectively.

Since its discovery in 2011,[16] black TiO_2 has been studied for its potential to quickly degrade a variety of pollutants, such as dyes, phenols, pesticides, pharmaceuticals, and others, using solar or visible light.[17,18] For instance, black TiO_2 produced by chemical reduction was able to completely degrade 20 mg/L of methyl orange in just 8 min of solar irradiation.[19] Another study reported 70% degradation of 30 mg/L Rhodamine B in just 5 min.[20] It is indisputable that black TiO_2 can swiftly degrade a variety of organic pollutants and enhance hydrogen production using solar light.[10,21−24] It can overcome the limitations of pristine TiO_2 through improved visible light absorption and lower photogenerated charge carrier recombination.[25] As an example, Vijayarangamuthu et al.[26] recently reported the production of black rutile TiO_2 with a crystalline core and an amorphous shell composed of Ti^{3+} species and Ti−OH bonding using microwave irradiation and H_2O_2. When compared to pure rutile TiO_2, H_2O_2-modified black TiO_2 demonstrated 3-fold greater photocatalytic performance for organic dye degradation. Sun et al.[27] used a hydrogenation

https://doi.org/10.1021/acsomega.3c04229
ACS Omega 2023, 8, 36076−36087

process with $NaBH_4$ as an H_2 source to prepare black TiO_2 with improved NIR and visible-light absorption. Naldoni et al.[18] have shed light on the specific structural and electronic characteristics of these catalytic materials, as well as the fundamental structure−activity correlations that govern the formation of crystal defects, enhanced light absorption, charge separation, and photocatalytic activity.

However, most of the synthetic techniques employed for the production of black TiO_2 use harsh synthesis conditions like high pressure and temperature, using expensive and toxic chemicals or reductants. Furthermore, in addition to their toxicity, the solvents and reductants used in these procedures are neither cheap nor easy to handle. In addition, because the reduction process occurs largely on the surface of TiO_2, the Ti^{3+} ions and surface oxygen vacancies (SOVs) produced by conventional hydrogenation procedures are typically unstable.

It is highly desirable to produce ZnO and black TiO_2 safely and use chemicals or solvents that are nontoxic, nonflammable, and widely accessible at a lower cost to satisfy the green chemistry principle. ZnO and TiO_2 are contenders in a variety of applications and have shown remarkable promise in wastewater treatment when modified with metals, nonmetals, organic coatings, and so on. However, modifying them with metals and other techniques does not always increase their performance under visible light nor does it always make the synthesis process sustainable. Previously, the viability of both photocatalysts for wastewater treatment was explored under UV light, and promising findings were found. However, it is also vital to study the efficacy of both systems in terms of wastewater treatment under visible light as this can make the process more economically viable. As a result, to the best of our knowledge, this is the first time that the performance of ZnO and black TiO_2 for the degradation of organic compounds has been extensively evaluated. In this study, green plant sources like *Polygonum minus* extract were used to synthesize ZnO. This plant species is widely available and is found throughout Malaysia. Utilizing an ionic-liquid-based technique with microwave assistance, the extract was obtained from *P. minus*. Due to its nontoxicity, low cost, and renewable nature, glycerol—which was used to produce black TiO_2—is regarded as environmentally friendly.[28] Glycerol is a by-product of biodiesel production, and its amount is expected to increase as various countries such as South America and Asian countries have a keen interest in biodiesel production. Therefore, incorporating excess glycerol in material synthesis provides the dual benefits of producing valuable materials while simultaneously eliminating the requirement to dispose of glycerol. The properties of the materials were determined using field emission scanning electron microscopy coupled with energy-dispersive X-ray spectroscopy, X-ray diffraction, ultraviolet−visible spectroscopy, Fourier transform infrared spectroscopy, and surface area and porosity measurements. The performance of the synthesized ZnO and black TiO_2 was evaluated for the degradation of two model compounds namely, MB and phenol.

MATERIALS AND METHODS

Materials. Ionic liquid 1-ethyl-3-methyl imidazolium acetate [C_3MIM][OAc], zinc nitrate hexahydrate ($Zn(NO_3)_3{\cdot}6H_2O$, titanium tetrachloride ($TiCl_4$, >99.9%), ammonium hydroxide (NH_4OH, 35%), glycerol (95%), phenol (>99%), and methylene blue were purchased from Merck. The plant was obtained from the local market of Malaysia. Distilled water was used throughout the experiments.

Extraction Procedure. The plant material was washed three times with distilled water to eliminate dust and dirt before being dried in the oven for 7 days at 45 °C. It was then ground and processed into a powder with a mesh size of 60−80 nm. Different powder sizes (20−40, 40−60, and 80−100) were employed, but 60−80 nm mesh exhibited higher extraction than others. First, the ionic liquid [C_3MIM][OAc] and powder were mixed in a 5:10 g/mL ratio and then transferred to a mantle balloon. For the extraction, a microwave operated at 50 °C and 60 W for 15 min was used. The microwave temperature was managed by an outside sensor. The extract was characterized using GCMS and FTIR spectroscopy and its chromatogram and spectrum are displayed in Figure 1.

The extract was chilled, filtered, and then stored at 4 °C in a refrigerator. The extract contains several bioactive compounds, as shown in Figure 1a, which play a vital role in the reduction of salts generally used for the synthesis of ZnO.

Synthesis of ZnO. For the synthesis of ZnO nanoparticles, 6 mL of extract was taken and heated for 5 min on a hot plate. Two grams of $Zn(NO_3)_2{\cdot}6H_2O$ were added to the extract and the reaction mixture was ultrasonicated. The reaction was completed in 8 min at 60 °C and 80 W. A yellow-colored paste was formed which floated on the surface of the solution. The paste was centrifuged at 4000 rpm for 10 min and separated from the aqueous ionic liquid. The paste was washed twice with distilled water to remove the impurities. The yellow precipitate was dried in a vacuum oven at 90 °C for 3 h. The powder was obtained and used for further analysis.

Synthesis of Black TiO_2. A modified precipitation method was used to prepare TiO_2 NPs, which involved hydrolyzing approximately 0.1 mol of $TiCl_4$ (purity >99.9%) in an aqueous glycerol solution (1.18 mol/L) under continuous stirring and then calcining it for an hour at 300 °C. Almost 300 mL of 2.5 M NH_4OH (purity, 35%) was added to the solution to complete the precipitation process. To help the $Ti(OH)_4$ sol settle as quickly as possible, produce the most precipitates possible, and stop mild nanoparticle aggregation from peptizing the solution, the pH was raised to 10. To recover and purify the precipitates, centrifugation was used at 10 000 rpm for 5 min. With distilled water, the precipitates were washed repeatedly until they were pH-neutral and chloride-free. The recovered precipitates were then dried at 60 °C for the following day. To create an anatase crystalline structure, TiO_2 was ground into fine particles and then calcined at 300 °C for 1 h.

Characterization of ZnO and Black TiO_2. The UV/vis spectrum of the nanoparticles was recorded in the range of 200−800 nm at 25 °C by using a Shimadzu UV spectrophotometer. The attenuated total reflection (ATR) spectrum of the nanoparticles was recorded by using an FTIR Nicolet 5700 spectrometer in the range of 800−4000 cm^{-1}. The solid sample was placed on a diamond crystal and pressed using a swivel presser tower. The crystal structure of nanoparticles was determined using a PANalytical XPERT-PRO X-ray diffractometer (XRD). The samples were scanned from 10 to 80° (2θ) at 24 °C with divergent receiving slots at 0.46° and 40 kV and 30 nA. The step size of 0.05° (2θ) and time of 10 s with continuous scanning were performed. The size of the crystallites was calculated using Scherrer's formula. The surface morphology of the nanoparticles was determined

https://doi.org/10.1021/acsomega.3c04229
ACS Omega 2023, 8, 36076−36087

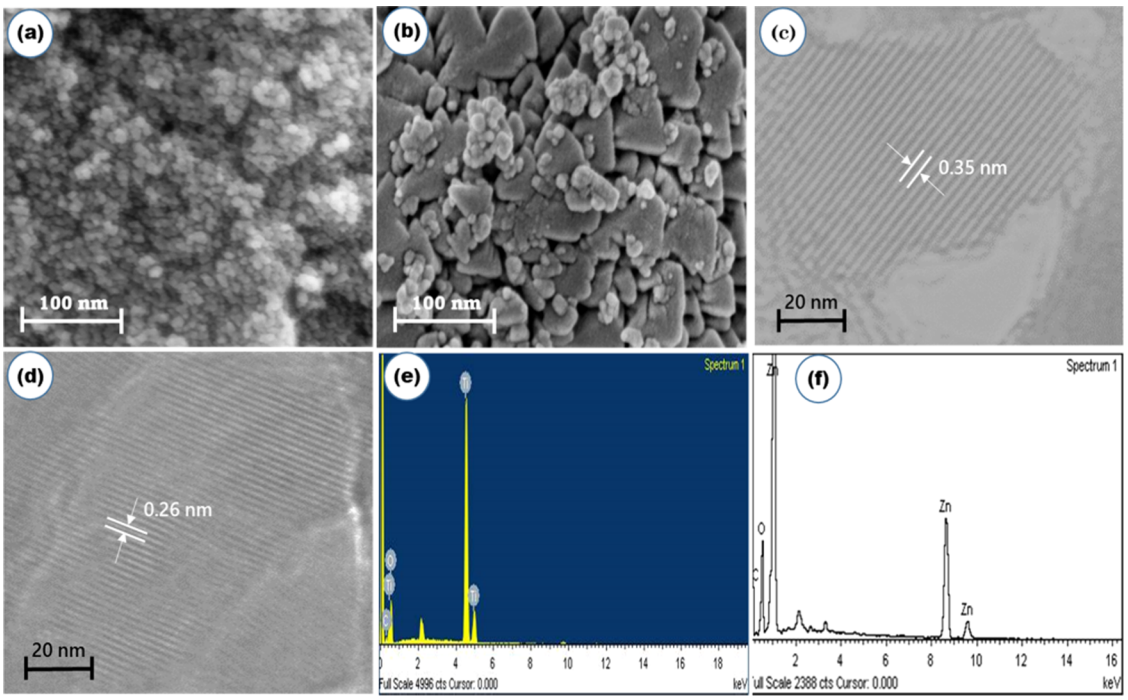

Figure 2. FESEM images showing the surface morphology of (a) TiO_2 and (b) ZnO; HRTEM images of (c) TiO_2 and (d) ZnO; EDX spectra displaying elemental composition of (e) TiO_2 and (f) ZnO.

by using a FESEM (Zeiss Supra 55VP). The samples were coated with gold water for conductivity before observation. The samples were also analyzed by EDX. HRTEM images were taken by using a transmission electron microscope (Tecnai G2-F20 X-Twin TMP). The materials' photoluminescence (PL) spectra were recorded by using a Horiba LabRam HR Evolution spectrometer. The sample for PL measurement was prepared according to the method given by Ishida et al.[29] At−196 °C, the samples' physiosorption isotherms were measured using a Micromeritics ASAP 2020 analyzer. Using the adsorption data, the specific surface area of the samples was calculated using the Brunauer−Emmett−Teller (BET) method. To estimate the pore size, the Barrett−Joyner−Halenda (BJH) method was applied.

Analytical Procedures. A stock solution of 5000 ppm of aqueous phenol was prepared by dissolving 0.25 g of phenol in 50 mL of deionized water. By serially diluting the stock solution, a standard phenol calibration curve (20−100 mg/L) was produced. Using a UV−vis spectrophotometer (Shimadzu UV-1280), we determined the concentration of phenol before and after treatment. The strongest absorbance peak at 270 nm was measured and compared to the calibration curve of the phenol standard. The degradation efficiency in terms of percentage removal of phenol was calculated based on the following equation (eq 1).

$$\text{degradation}\,(\%) = \frac{C_{\text{initial}} - C_{\text{final}}}{C_{\text{initial}}} \times 100\% \quad (1)$$

where C_{initial} is the phenol concentration before treatment and C_{final} is the phenol concentration following treatment at various intervals.

A stock solution containing 5000 ppm of MB was prepared by dissolving 0.25 g of MB in 50 mL of deionized water. A standard calibration curve (20−100 mg/L) of aqueous MB was prepared using serial dilutions. A UV−vis spectrophotometer was used to measure MB absorption (Shimadzu UV-1280). The highest absorbance peak at 668 nm was compared to the calibration curve of the MB standard for the determination of the MB concentration before and after the treatment. The degradation efficiency in terms of percentage removal of MB was calculated based on eq 1.

Photocatalytic Activity Assessment. The performance of both types of materials—ZnO and black TiO_2, was evaluated for photodegradation of MB and phenol under visible light irradiation. The reactions were carried out in batch mode in a 150 mL glass reactor. A fixed amount of ZnO and black TiO_2 was dispersed to make 0.2 g/L of photocatalyst concentration in 50 mL of phenol and MB solution with initial concentrations of 40 mg/L. To achieve adsorption−desorption equilibrium, the suspension was thoroughly stirred for 20 min in the dark. Then, to power the reactions, a 150 W halogen lamp was turned on to deliver visible light. The reaction was run for a total of 60 min while samples were taken from the reactor at regular intervals. The samples were immediately passed through a 0.45 μm Whatman filter to remove the residual solid particles before UV analysis.

Kinetic Investigations. To further evaluate the performance of ZnO and black TiO_2 for degradation of MB and phenol, kinetic investigations were carried out. Pseudo-first-order kinetics as shown in eqs 2 and 3 can be used to describe how ZnO and black TiO_2 degrade phenols through photocatalysis.

$$d = -\frac{dC_t}{d_t} = kC_t \quad (2)$$

$$\ln\left(\frac{C_0}{C_t}\right) = kt \quad (3)$$

https://doi.org/10.1021/acsomega.3c04229
ACS Omega 2023, 8, 36076−36087

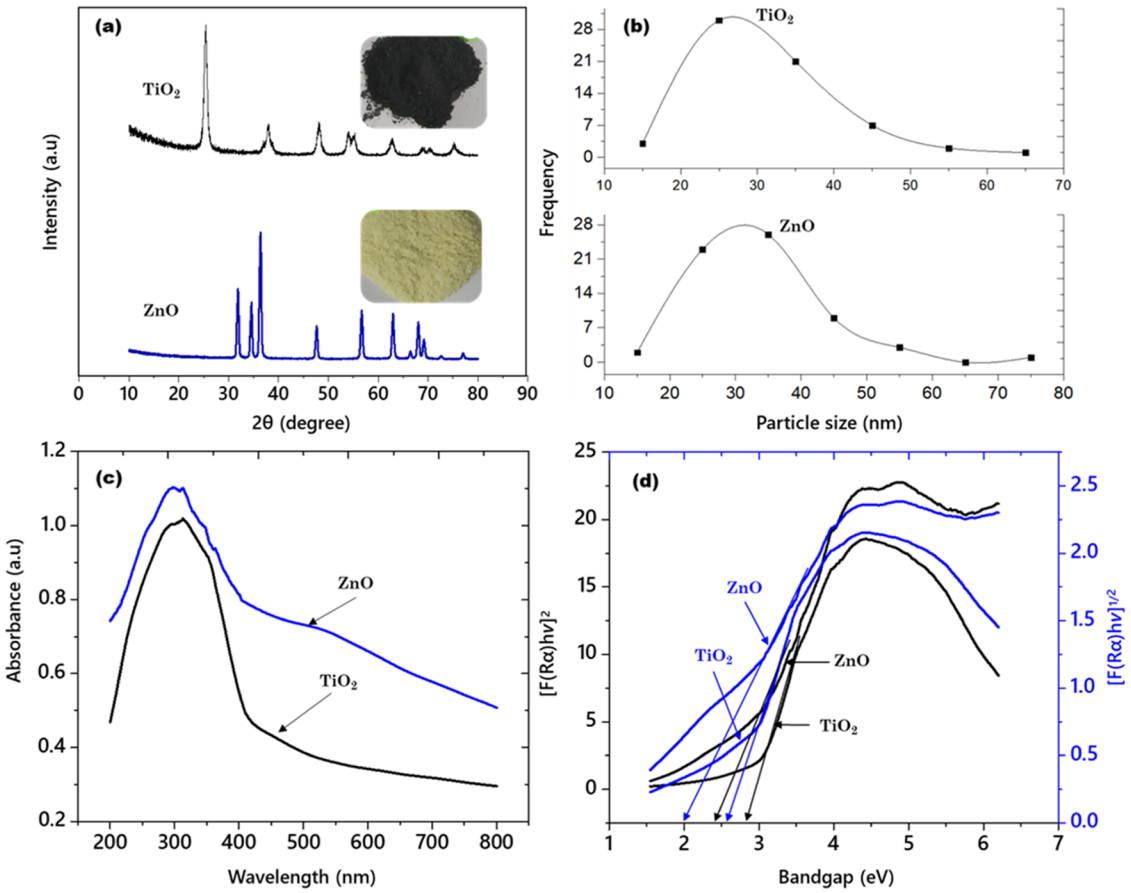

Figure 3. (a) XRD diffractogram, (b) particle size distribution, (c) UV−visible spectra, and (d) Tauc's plot of the band gap of ZnO and TiO_2.

where C_0 is the initial concentration of phenol and MB, C_t is the phenol and MB concentration at a given time (t), and d is the degradation rate constant.

RESULTS AND DISCUSSION

Comparison of Properties of ZnO and Black TiO_2. At 100k× magnification, FESEM images of ZnO and black TiO_2 were captured, and the differences in the surface and morphology of the two materials were examined. Both materials are spherical in shape, as shown by a comparison of the surface images of black TiO_2 in Figure 2a and ZnO in Figure 2b. However, ZnO presented a few particles with irregular shapes. The slight agglomeration of both types of particles may be caused by electrostatic interaction and polarity.[30] While black TiO_2 particles were uniformly distributed, the ZnO particles were unevenly distributed and clustered.

By choice of random particles from the FESEM images, the particle sizes of the two materials were calculated. The particle size distribution of the materials is shown in Figure 3b. ZnO has average particles that were 32 nm in average size as opposed to 28 nm in black TiO_2. Larger-sized particles typically result from biomass-mediated synthesis.[31] Its larger size may be due to the clustered nature of ZnO particles (Figure 2b), whose higher surface energies cause densification due to the constrained space between the compounds in *P. minus*. Research indicates that the particle size determined by DLS typically represents the hydrodynamic size of the particle, which is said to be larger than the actual size of the particles.[32]

HRTEM images were obtained to investigate the structural properties and atomic arrangement in synthesized ZnO and black TiO_2. HRTEM micrographs are displayed in Figure 2. Figure 2c shows black TiO_2 with well-resolved lattice features and distinct lattice fringes. The lattice spacing of d is 0.35 nm, which can be ascribed to the interplanar distance of the anatase (101) plane based on the distance between neighboring lattice fringes. The HRTEM image of ZnO shown in Figure 2d revealed that the interplanar distance between the lattice atoms is 0.26 nm, which corresponds to the wurtzite structure. HRTEM results are consistent with the XRD results shown in Figure 3a.

One peak in the EDX spectrum of black TiO_2 shown in Figure 2e confirms the presence of the Ti element, and the other peak is associated with the O atom validating the formation of TiO_2. The EDX spectrum of ZnO in Figure 2f primarily shows two components that are attributed to the Zn and O elements that make up the ZnO compound. In both instances, a second C peak can be seen; in ZnO, it is apparent due to bioactive compounds,[33] whereas in black TiO_2, it may be due to glycerol.[34]

Crystal structures of ZnO and black TiO_2 were analyzed using XRD. Figure 3a displays the XRD diffractograms of the materials. The diffraction peaks showed that black TiO_2 has an anatase structure according to JCPDS card no. 21-1272[35] while ZnO has a wurtzite structure based on JCPDS card no. 36-1451.[36] In reality, TiO_2 was black in color, as illustrated in the inset of Figure 3a, which can be used to evaluate the production of black TiO_2. The intense diffraction peaks of both samples indicate that they are highly crystalline. The

https://doi.org/10.1021/acsomega.3c04229
ACS Omega 2023, 8, 36076−36087

nanoparticles were grown preferentially in the (101) crystal plane direction, as indicated by the narrow and intense diffraction peaks at 2θ (25.46°) in black TiO_2 and 36.41° in ZnO.

Both materials (ZnO and black TiO_2) were subjected to UV−visible spectroscopy analyses to gain knowledge about their optical characteristics. The UV−vis absorbance spectra of the samples are shown in Figure 3c. As can be seen, ZnO outperformed black TiO_2 as a more effective light absorber in the visible range. However, both types of materials have a greater capacity to absorb visible light than their equivalents found commercially. The introduction of defect states (primarily Ti^{3+} cations) through reduction with glycerol, as previously demonstrated,[37] may be the cause of the increased visible light absorbance capacity of black TiO_2. It was suggested that the biocomponents present in the *P. minus* extract used during its synthesis were the reason for improved visible light absorption by ZnO. According to reports, these biocomponents improve the general as well as optical properties of ZnO.[38] Using the absorbance data, the direct and indirect band gaps (E_g) of ZnO and black TiO_2 were calculated and listed in Table 1. E_g was calculated using Tauc's

Table 1. Properties and Performance of ZnO and Black TiO_2 NPs

properties	ZnO	black TiO_2
E_g (eV), direct	2.46	2.85
E_g (eV), indirect	1.98	2.67
particle size (nm)	25	10
surface area (m^2/g)	353.11	239.99
pore volume (m^3/g)	0.0196	0.1922
pore size (nm)	2.8952	3.5373
MB degradation (%)	97.50	90.00
MB degradation rate constant ($kmin^{-1}$)	3.6888	2.3025
MB degradation (R^2)	0.9765	0.9897
phenol degradation (%)	75.15	61.05
phenol degradation rate constant ($kmin^{-1}$)	1.3923	0.9428
phenol degradation (R^2)	0.9865	0.9846

methods, as shown in Figure 3d. ZnO has a direct and indirect E_g of 2.65 and 1.98 eV, respectively, which is lower than that of black TiO_2 (2.85 and 2.46 eV). Again, both synthesized materials have E_g lower than that of the commercially available ZnO and TiO_2. Similar to light absorbance, the E_g of both synthetic materials is lower than that of ZnO and TiO_2, which are readily available in the market. Previous studies that tuned the optical properties of ZnO and TiO_2 using metals, nonmetals, and other dopants have demonstrated this narrowing of E_g; however, in this study, the optical properties were altered *in situ*.

FTIR was used to examine the black TiO_2 and ZnO materials. The FTIR spectra of both samples are displayed in Figure 4a. Both the samples exhibit a broad peak at around 3400 cm^{-1} demonstrating the stretching vibrations of the hydroxyl (O−H) of alcohol (glycerol) used in the synthesis of black TiO_2 and bioactive compounds from *P. minus* extract used in the synthesis of ZnO. An extra peak at 1400 cm^{-1} can be observed in the FTIR spectrum of ZnO, which arises from primary amines.[32] Zinc nitrate is reduced to zinc oxide due to the abundance of OH groups in polyphenols and flavonoids extracted from plant biomass. The peak at 458 cm^{-1} is due to the stretching vibration of zinc oxide. It is known that polyphenols and flavonoids extracted from plant biomass can bind to the Zn surface in $ZnHNO_3$ and result in the formation of ZnO.[39] In the FTIR spectrum of black TiO_2, the peak is around 700 cm^{-1} illustrating the stretching vibration of Ti−O oxide.[40]

Surface area and porosity measurements were used to determine the textural characteristics of ZnO and black TiO_2. In Figure 4b, the N_2 adsorption and desorption isotherms of the materials are displayed. Type IV isotherms with the H_2 type hysteresis loop, which were examined, showed that black TiO_2 has a mesoporous nature. When the relative pressure is between 0.4 and 0.8, the desorption branch typically rises. Additionally, the desorption branch is steeper than the adsorption branch, indicating that capillary condensation occurs first, then a monolayer forms within the pores.[41] On the other hand, ZnO displays a H_1 hysteresis loop and type III isotherms. In the hysteresis loop, ZnO has equal adsorption and desorption branches. According to isotherm analysis, the pore structures of black TiO_2 and ZnO have very different textures. Black TiO_2 has cylindrically shaped pores, whereas ZnO has ink-bottle-shaped pores. As shown in Table 1, the specific surface area of ZnO is 353.11 m^2/g, nearly 48% more than that of black TiO_2 (239.99 m^2/g). This might be a result of the presence of irregular pores with variable pore sizes and equal entrance diameters.[41] ZnO has a narrow pore size of 2.8952 nm compared to 3.5373 nm of black TiO_2.

The photocatalytic activity of photocatalysts is dependent on the duration of excited electrons and holes in their outermost layer before they are consumed by recombination. To investigate the behavior of electron−hole pair recombination, the photoluminescence (PL) spectra of ZnO and black TiO_2 were examined. The PL of ZnO and black TiO_2 was measured at wavelengths ranging from 300 to 700 nm, using excitation at 325 nm. Figure 4c indicates that the PL peak intensities of the ZnO were substantially lower than those of black TiO_2, implying that the ZnO has less electron and hole recombinations. Higher peak intensities indicate stronger electron−hole pair recombination and shorter lifetimes in charged species.[42]

Photocatalytic Degradation of Organic Pollutants. To assess the performance of ZnO and black TiO_2, MB and phenol were used as model substrates. MB and phenol were considered because both of these pollutants are resistant to physicochemical and biological treatments. In addition, they are most widely found in industrial wastewater.[43] The change in the maximum absorbance peak, which is located at 668 nm, was used to track the degradation of MB. As can be seen in Figure 5a, the peak intensity of MB in the presence of ZnO under visible light significantly decreased with reaction time. With a degradation rate constant of 3.6888 $kmin^{-1}$, 97.50% of 40 mg/L MB was degraded within 60 min of exposure to visible light as shown in Figure 5d. The extreme viability of the green synthesized ZnO for the degradation of organic dyes was suggested by the fact that the MB concentration in aqueous solution was decreased from 40 to only 0.5 mg/L in 60 min.

It should be noted that there was hardly any change in the MB peak position, indicating that the pollutant was completely mineralized without the formation of any significant intermediates. However, as can be seen in Figure 5c, black TiO_2 could only degrade 90.00% of MB in the same amount of time as ZnO. Their degradation rate constants show another important distinction between black TiO_2 and ZnO in terms of performance. In the presence of ZnO, the degradation rate

https://doi.org/10.1021/acsomega.3c04229
ACS Omega 2023, 8, 36076−36087

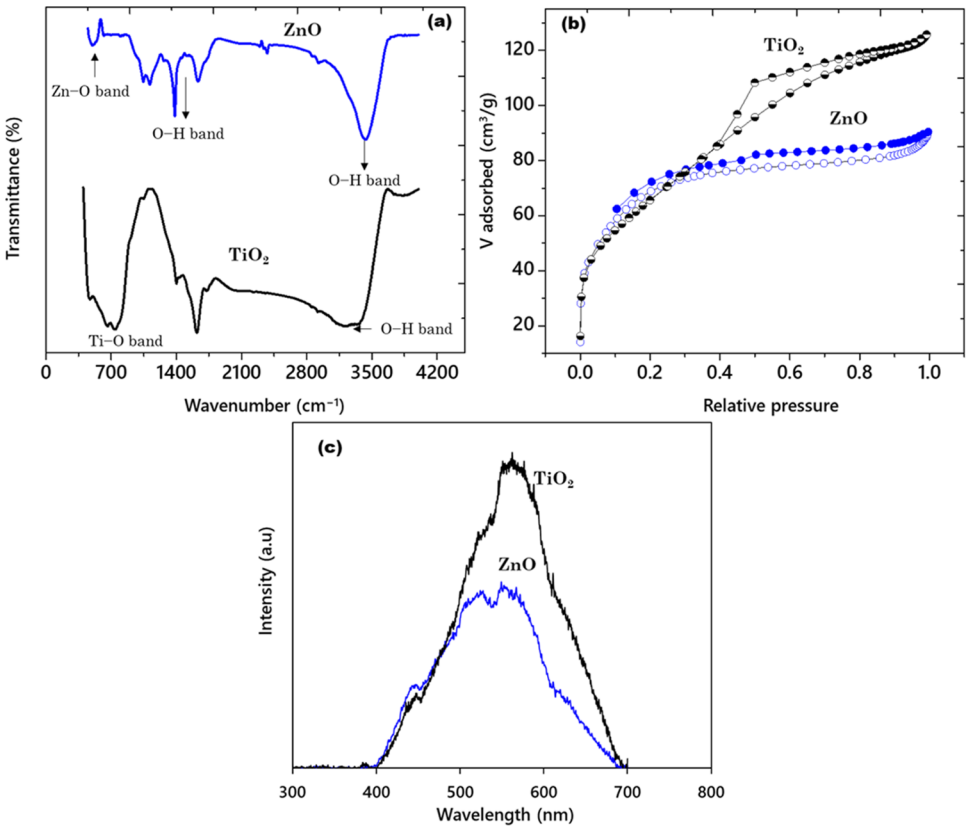

Figure 4. (a) FTIR spectra, (b) N_2 adsorption and desorption isotherms, and (c) PL spectra of ZnO and TiO_2.

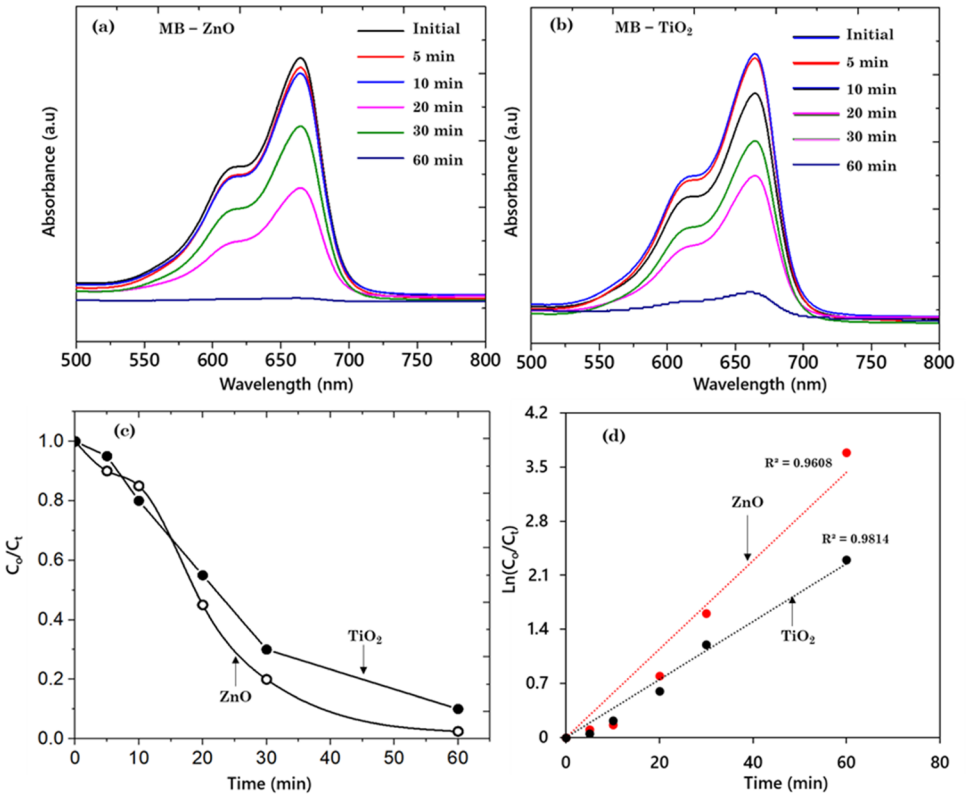

Figure 5. Visible absorbance spectra of MB after 60 min of photocatalytic treatment with (a) ZnO and (b) TiO_2, (c) normalized concentration and percentage degradation of MB, and (d) pseudo-first-order kinetics of MB degradation by ZnO and TiO_2.

https://doi.org/10.1021/acsomega.3c04229
ACS Omega 2023, 8, 36076−36087

constant of MB was greater than that of black TiO_2 as shown in Figure 5d. Black TiO_2 displayed a degradation rate constant of 2.3025 $kmin^{-1}$ as opposed to 3.6888 $kmin^{-1}$. There are two possible explanations for the improved performance of ZnO. First, ZnO is said to have higher charge mobility (200−300 $cm^2/(V\ s)$) than TiO_2 (only 0.1−0.4 $cm^2/(V\ s)$).[44] Second, ZnO has a surface area of 353.11 m^2/g, which is significantly higher than that of black TiO_2 (239.99 m^2/g). Additionally, through Förster resonance energy transfer, the emission energy from the ZnO analogue might also accelerate the efficient degradation of MB.[45] A significant spectral overlap between the ZnO emission spectrum and the MB absorption spectrum is necessary for the effective photocatalytic degradation of MB. To obtain the emission spectra, ZnO was excited at 325 nm. When the ZnO emission spectrum in Figure 3c is compared to the MB absorption spectrum in Figure 4a, it is clear that there is a large spectral overlap between one of the ZnO emissions and the MB absorption at 600−700 nm. This energy overlap is responsible for ZnO's superior photocatalytic efficiency over black TiO_2.[45,46]

ZnO has also shown less recombination of electrons and holes as shown in Figure 4c, which could be another reason for the enhanced performance of the material. Importantly, compared with earlier studies, black TiO_2 synthesized in the current study performs better in terms of MB degradation. Anodized black TiO_2 nanotubes have been reported in earlier studies to only degrade 60% of 10 mg/L MB when exposed to visible light from a 300 W lamp.[47] There is undoubtedly a trade-off; earlier research was able to degrade MB and produce energy in the form of hydrogen simultaneously, whereas in the current work only MB was degraded but faster than the anodized black TiO_2 nanotubes.

In another instance, 95.2% of MB was degraded under simulated solar light using cerium-doped ZnO.[48] However, doping metals or nonmetals into the lattice of either ZnO or TiO_2 can make their production process costly. The impact of metal ion dopants on the efficiency of the photocatalytic reaction is a complicated phenomenon. The effect on the photocatalytic performance of TiO_2 doped with different metals or the same metal by using various techniques is not the same. For instance, zinc (Zn)-doped TiO_2 was synthesized using sol−gel and combustion techniques, and its effectiveness in degrading phenol was assessed. Comparing the results, it can be seen that combustion-produced Zn/TiO_2 only removed 45% of the phenol, whereas Zn/TiO_2 prepared via the sol−gel method removed 76% of phenol.[49,50] Contrarily, Zn/TiO_2 and iron (Fe)-doped TiO_2 samples were synthesized using the same procedure (sol−gel), and their efficacy for the degradation of phenol was tested. The findings show that Zn/TiO_2 has a higher phenol removal efficiency (76%) than Fe/TiO_2 (48%).[51] Thus, doping ZnO or TiO_2 with metals or nonmetals is somehow not favorable for tuning their optical characteristics.

Additionally, the effectiveness of ZnO and black TiO_2 was evaluated against other comparable studies. In just 10 min of exposure to visible light from a 300 W Halogen lamp (Osram Tungsten), the ZnO/TiO_2 composite synthesized using *C. mucunoides* extract was reported to degrade 98.36% of Congo red. Despite having a green origin, the composite was calcined at 800 °C for 2 h, which can be viewed as an energy-intensive process. Furthermore, 5 g of the material was used in photoreactions, which can be viewed as a chemically intensive process. In contrast to the previous study, the amount of material used in the current work −0.2 g/L is quite low.[11]

Additionally, the performance of synthesized ZnO and black TiO_2 was evaluated for the degradation of phenol. The normalized concentration and percentage degradation of phenol after 60 min of visible light reaction is shown in Figure 6a. Both materials' efficacy is decreased when tested for

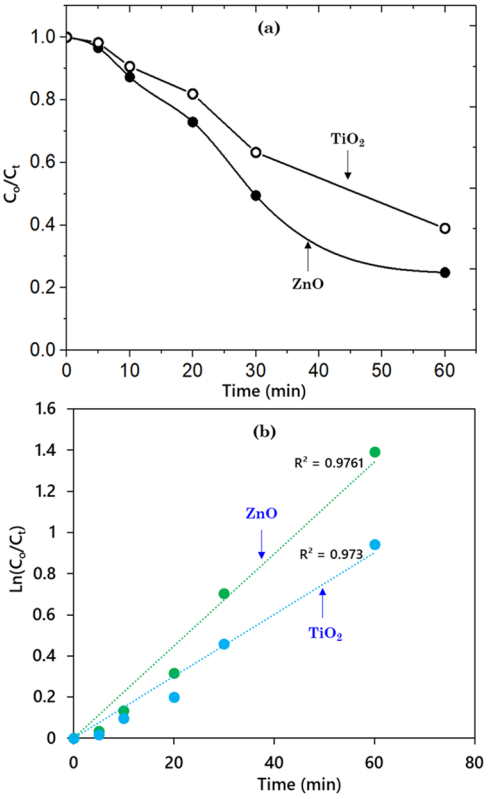

Figure 6. (a) Normalized concentration and percentage degradation of phenol and (b) pseudo-first-order kinetics of phenol degradation by ZnO and TiO_2.

phenol degradation as opposed to MB degradation. In comparison to 61.05% by black TiO_2, ZnO reduced the concentration of phenol by 75.15% in just 60 min. ZnO had a phenol degradation rate constant of 1.3923 as opposed to MB's 3.6888 $kmin^{-1}$. Similar to this, the degradation rate constant of black TiO_2 for phenol was 0.9428 compared to 2.3025 min^{-1} for MB degradation (Figure 6b). The acidic nature of phenol, which results from its capacity to lose hydrogen ions to form phenoxide ions, may be the cause of the reduction in the performance of ZnO and black TiO_2. It is reasonable to assume that phenol solution is more acidic than MB solution, which can affect the adsorption of organic molecules on the surface of both photocatalysts and change the surface of both.[52] The pH of the solution caused a difference between ZnO and black TiO_2 for the degradation of MB and phenol, because photocatalysis is a surface phenomenon and pH alters the surface properties.

Photocatalytic Degradation Mechanism of MB over ZnO. An explanation for the plausible mechanism of the degradation of MB over ZnO under visible light is provided based on previously reported and study-specific results.[53] The degradation mechanism and pathway of MB are shown in Figure 7. The electrons in the valence band of ZnO are ejected

https://doi.org/10.1021/acsomega.3c04229
ACS Omega 2023, 8, 36076−36087

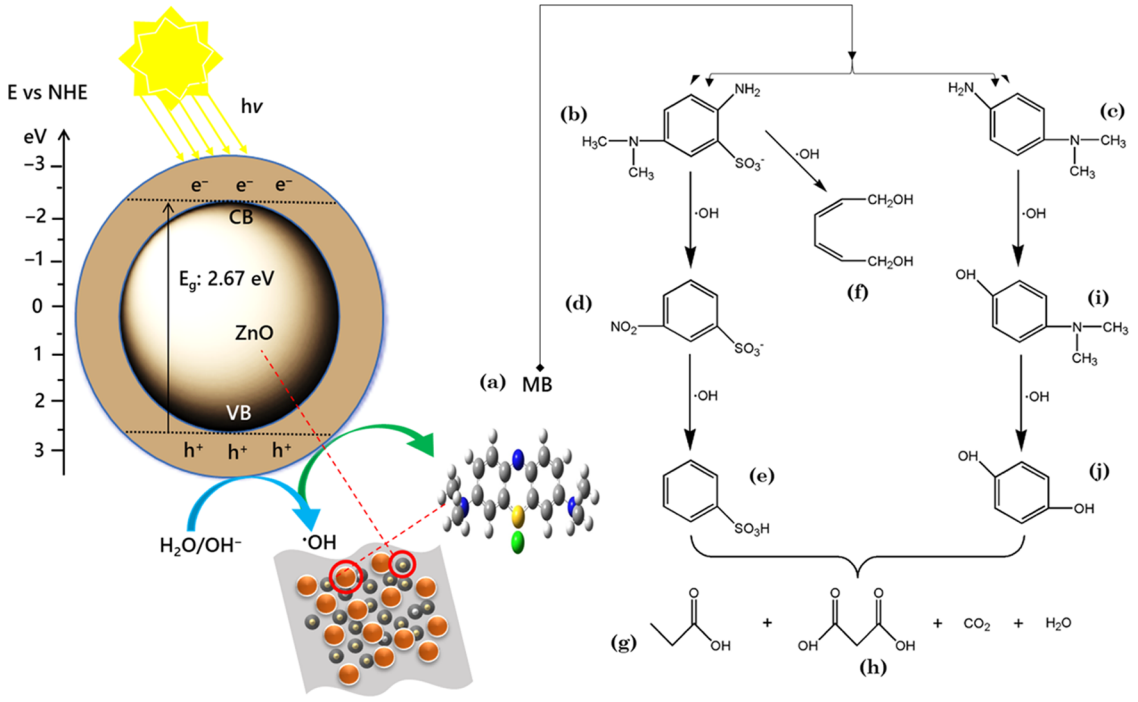

Figure 7. Photocatalytic degradation mechanism of MB over ZnO under visible light irradiation; (a) MB, (b) 2-amino-4-(*N*,*N*-dimethyl)-benzenesulfonic acid, (c) 4-(*N*,*N*-dimethyl)-aniline, (d) *p*-nitrobenzenesulfonic acid, (e) benzenesulfonic acid, (f) 2,4-hexadiene-1,6-diol, (g) propionic acid, (h) malonic acid, (i) 4-(*N*,*N*-dimethyl)-phenol, and (j) hydroquinone.

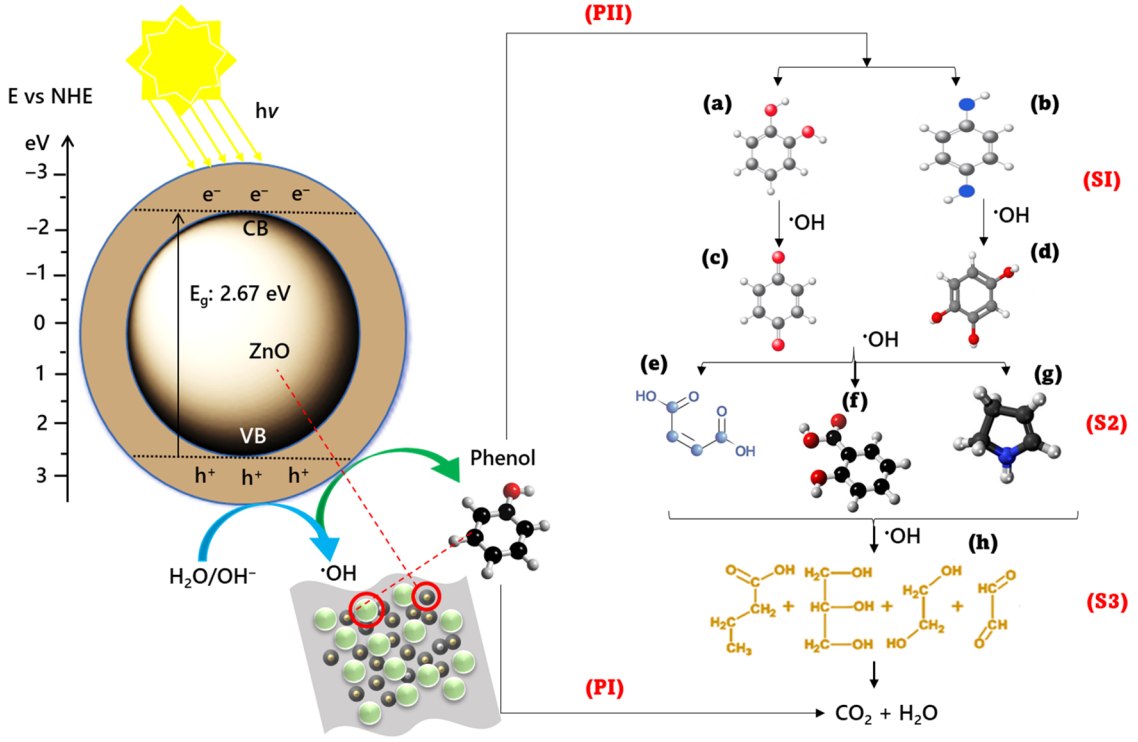

Figure 8. Photocatalytic degradation mechanism of phenol over ZnO under visible light irradiation; (a) hydroquinone, (b) catechol, (c) benzoquinone, (d) benzene-1.2.3-triol, (e) maleic acid, (f) salicylic acid, (g) 2-propylphenol, and (h) carboxylated and hydroxylated organic chain.

when it is exposed to visible light, moving them to the conduction band where they are free to participate in photoreactions unless they recombine. At the same time, holes are generated in the valence band. While the holes on the VB react with $^{\bullet}OH^-$ to produce $^{\bullet}OH$, the electrons in the CB react with O_2 to produce $^{\bullet}O_2^-$. Both of these species are reactive and attack MB molecules.[43]

Initially, the $^{\bullet}OH$ attacked the sulfur and nitrogen conjugated system (a) in the MB molecule and converted it into 2-amino-4-(*N*,*N*-dimethyl)-benzenesulfonic acid (b) and 4-(*N*,*N*-dimethyl)-aniline (c). The remaining "b" then under-

https://doi.org/10.1021/acsomega.3c04229
ACS Omega 2023, 8, 36076−36087

goes a series of reactions to produce 2,4-hexadiene-1,6-diol (f), which cannot be further broken down until the end of the reaction. The other portion of "b" is oxidized to form *p*-nitrobenzenesulfonic acid (d) following further oxidation to form benzenesulfonic acid (e). The simultaneous oxidation and deamination of "c" results in the formation of 4-(*N*,*N*-dimethyl)-phenol (i), which is then oxidized to form hydroquinone (j). Small organic molecules propionic acid (g) and malonic acid (h) are produced when •OH attacks a portion of the resulting intermediates "e" and "j". The remaining intermediates undergo oxidation, which produces several smaller molecules, such as CO_2 and H_2O.

Photocatalytic Degradation Mechanism of Phenol over ZnO. Phenol degradation proceeds with a different pathway in the presence of different photocatalysts. In light of this, we carefully reviewed several articles and dissertations on the mechanism of phenol photodegradation and discovered a widely recognized mechanism.[54−56] A possible mechanism of phenol degradation over ZnO under visible light is shown in Figure 8. In general, phenol is degraded through three different processes. However, here are the two pathways that are most relevant and discussed as follows. A direct ring-opening reaction first breaks down the phenol, converting it into carbon dioxide and water (pathway I). The second (pathway II) is that phenol first goes through oxidation to create p-benzoquinone, and then ring-opening reactions occur, causing p-benzoquinone to mineralize into carbon dioxide and water by the transformation of intermediates.[57] In PII, the phenol molecule is converted into hydroquinone (a) and catechol (b) in the first step (SI). In step 1, "a" is further broken down to benzoquinone (c), whereas "b" is converted into benzene-1,2,3-triol (d). This is followed by step SII, where "c" and "d" are converted to maleic acid (e), salicylic acid (f), and 2-propylphenol (g), and then "e", "f", and "g" are converted to carboxylated and hydroxylated organic chain (h). "h" is finally mineralized into water and carbon dioxide.[54]

CONCLUSIONS

Environmentally friendly and sustainable solution routes utilizing *P. minus* extract and glycerol were adopted for the synthesis of ZnO and black TiO_2. Both materials were nanosized materials with typical anatase and hexagonal wurtzite structures, respectively. In terms of photocatalytic degradation of organic pollutants, ZnO outperformed black TiO_2 with 99.50% MB degradation versus 90.00% for black TiO_2 in 60 min of treatment time under visible light. Similarly, when tested for phenol degradation, ZnO also performed better than black TiO_2 suggested by 75.15% degradation of phenol compared to only 61.05% by black TiO_2. According to this study, ZnO can be prepared via microwave-assisted ionic-liquid-based extraction of *P. minus* extract and has superior capabilities for the photocatalytic degradation of organic pollutants. The better performance of ZnO was attributed to its lower band gap and rate of electron and hole recombination.

AUTHOR INFORMATION

Corresponding Author

Rab Nawaz − *Institute of Soil and Environmental Sciences, Pir Mehr Ali Shah Arid Agriculture University Shamsabad, 46300 Rawalpindi, Pakistan; Department of Earth Sciences and Environment, Faculty of Science and Technology, Universiti Kebangsaan Malaysia (UKM), 43600 Bangi, Selangor, Malaysia; Centre for Research and Instrumentation Management (CRIM), Universiti Kebangsaan (UKM), 43600 Bangi, Selangor, Malaysia;* orcid.org/0000-0001-7528-8094; Email: rabnawaz.utp@gmail.com

Authors

Habib Ullah − *Fundamental and Applied Sciences (FASD), Universiti Teknologi PETRONAS (UTP), 32610 Seri Iskandar, Perak, Malaysia*

Abdulnoor Ali Jazem Ghanim − *Civil Engineering Department, College of Engineering, Najran University, Najran 61441, Saudi Arabia*

Muhammad Irfan − *Electrical Engineering Department, College of Engineering, Najran University, Najran 61441, Saudi Arabia;* orcid.org/0000-0003-4161-6875

Muzammil Anjum − *Institute of Soil and Environmental Sciences, Pir Mehr Ali Shah Arid Agriculture University Shamsabad, 46300 Rawalpindi, Pakistan;* orcid.org/0000-0002-5955-0053

Saifur Rahman − *Electrical Engineering Department, College of Engineering, Najran University, Najran 61441, Saudi Arabia*

Shafi Ullah − *Institute of Soil and Environmental Sciences, Pir Mehr Ali Shah Arid Agriculture University Shamsabad, 46300 Rawalpindi, Pakistan*

Zaher Abdel Baki − *College of Engineering and Technology, American University of the Middle East, Egaila 15453, Kuwait*

Vipin Kumar Oad − *Faculty of Civil and Environmental Engineering, Gdansk University of Technology, 80-233 Gdansk, Poland*

Complete contact information is available at: https://pubs.acs.org/10.1021/acsomega.3c04229

Notes

The authors declare no competing financial interest.

ACKNOWLEDGMENTS

The authors acknowledge the Deanship of Scientific Research, Najran University, Kingdom of Saudi Arabia for funding this work under the Research Groups Funding Program grant code number NU/RG/SERC/12/15.

REFERENCES

(1) Bhunia, P.; Dutta, K.; Vadivel, S. *Photocatalysts and Electrocatalysts in Water Remediation: From Fundamentals to Full Scale Applications*; Wiley: New York, 2023.

(2) Sun, W.; Guo, R.; Shi, C.; Li, X.; Wu, J.; Tian, H.; Hauyi, L.; Jei, H.; Zhengchun, Y.; Jiahui, L.; Shanfeng, S. Preparation and Photocatalytic Properties of CQDs-Modified 26-Facet Cu/Cu_2O Composites. *Catal. Lett.* **2023**, DOI: 10.1007/s10562-023-04344-9.

(3) Dai, H.; Wang, C.; Cai, X.; Li, X.; Jiang, G.; Wei, R. First-Principles Calculations on the HER Performance of TiO_2 Nanosheet with Passivated Codoping. *Catal. Lett.* **2023**, *153*, 1278−1283.

(4) Sakthivel, S.; Neppolian, B.; Shankar, M. V.; Arabindoo, B.; Palanichamy, M.; Murugesan, V. Solar photocatalytic degradation of azo dye: comparison of photocatalytic efficiency of ZnO and TiO_2. *Sol. Energy Mater. Sol. Cells* **2003**, *77*, 65−82.

(5) Jandaghian, F.; Pirbazari, A. E.; Tavakoli, O.; Asasian-Kolur, N.; Sharifian, S. Comparison of the performance of Ag-deposited ZnO and TiO_2 nanoparticles in levofloxacin degradation under UV/visible radiation. *J. Hazard. Mater. Adv.* **2023**, *9*, No. 100240.

(6) Ng, K. H.; L Yuan, L. S.; Cheng, C. K.; Chen, K.; Fang, C. TiO_2 and ZnO photocatalytic treatment of palm oil mill effluent (POME)

and feasibility of renewable energy generation: A short review. *J. Cleaner Prod.* **2019**, *233*, 209−225.
(7) Wang, X.; Qiao, P.; Chen, Q.; Dai, M.; Liu, Y.; Wang, Y.; Wang, W.; Liu, Y.; Song, H. Electrochemically Deposited Cu_2O-Doped TiO_2 Nanotube Photoanodes for Hydrogen Evolution. *Catal. Lett.* **2023**, *153*, 1689−1695.
(8) Gandhi, S.; Sharma, V.; Koul, I. S.; Mandal, S. K. Shedding Light on the Lewis Acid Catalysis in Organic Transformations Using a Zn-MOF Microflower and Its ZnO Nanorod. *Catal. Lett.* **2023**, *153*, 887−902, DOI: 10.1007/s10562-022-04004-4.
(9) Jandaghian, F.; Ebrahimian Pirbazari, A.; Tavakoli, O.; Asasian-Kolur, N.; Sharifian, S. Comparison of the performance of Ag-deposited ZnO and TiO_2 nanoparticles in levofloxacin degradation under UV/visible radiation. *J. Hazard. Mater. Adv.* **2023**, *9*, No. 100240.
(10) Kumbhakar, P.; Biswas, S.; Kumbhakar, P. Observation of high photocatalytic activity by tuning of defects in chemically synthesized ethylene glycol capped ZnO nanorods. *Optik* **2018**, *154*, 303−314.
(11) Rusman, E.; Heryanto, H.; Fahri, A. N.; Rahmat, R.; Mutmainna, I.; Tahir, D. Green synthesis ZnO/TiO_2 for high recyclability rapid sunlight photodegradation wastewater. *MRS Adv.* **2022**, *7*, 444−449.
(12) Cheng, C. K.; Deraman, M. R.; Ng, K. H.; Khan, M. R. Preparation of titania doped argentum photocatalyst and its photoactivity towards palm oil mill effluent degradation. *J. Cleaner Prod.* **2016**, *112*, 1128−1135.
(13) Cheng, C. K.; Derahman, M. R.; Khan, M. R. Evaluation of the photocatalytic degradation of pre-treated palm oil mill effluent (POME) over Pt-loaded titania. *J. Environ. Chem. Eng.* **2015**, *3*, 261−270.
(14) Kumbhakar, P.; Pramanik, A.; Biswas, S.; Kole, A. K.; Sarkar, R.; Kumbhakar, P. In-situ synthesis of rGO-ZnO nanocomposite for demonstration of sunlight driven enhanced photocatalytic and self-cleaning of organic dyes and tea stains of cotton fabrics. *J. Hazard. Mater.* **2018**, *360*, 193−203.
(15) Mohamed, R. M.; Ismail, A. A.; Kadi, M. W.; Alresheedi, A. S.; Mkhalid, A. I. Photocatalytic performance mesoporous Nd_2O_3 modified ZnO nanoparticles with enhanced degradation of tetracycline. *Catal. Today* **2020**, *380*, 259−267, DOI: 10.1016/j.cattod.2020.11.002.
(16) Chen, X.; Liu, L.; Peter, Y. Y.; Mao, S. S. Increasing solar absorption for photocatalysis with black hydrogenated titanium dioxide nanocrystals. *Science* **2011**, *331*, 746−750.
(17) Hu, M.; Meng, F.; Li, N.; Zhang, S.; Ma, J. Insight Into the CuO_x Interacts with Oxygen Vacancies on the Surface of Black-TiO_2 for NO Oxidation. *Catal. Lett.* **2022**, *152*, 2869−2879.
(18) Naldoni, A.; Altomare, M.; Zoppellaro, G.; Liu, N.; Kment, S.; Zboril, R.; Schmuki, P. Photocatalysis with Reduced TiO_2: From Black TiO_2 to Cocatalyst-Free Hydrogen Production. *ACS Catal.* **2019**, *9*, 345−364.
(19) Wang, H.; Lin, T.; Zhu, G.; Yin, H.; Lü, X.; Li, Y.; Huang, F. Colored titania nanocrystals and excellent photocatalysis for water cleaning. *Catal. Commun.* **2015**, *60*, 55−59.
(20) Bi, X.; Du, G.; Sun, D.; Zhang, M.; Yu, Y.; Su, Q.; Ding, S.; Xu, B. Room-temperature synthesis of yellow TiO_2 nanoparticles with enhanced photocatalytic properties. *Appl. Surf. Sci.* **2020**, *511*, No. 145617.
(21) Bi, Q.; Huang, X.; Dong, Y.; Huang, F. Conductive Black Titania Nanomaterials for Efficient Photocatalytic Degradation of Organic Pollutants. *Catal. Lett.* **2020**, *150*, 1346−1354.
(22) Wang, C.; Kang, X.; Liu, J.; Wang, D.; Wang, N.; Chen, J.; Wang, J.; Tian, C.; Fu, H. Ultrathin black TiO_2 nanosheet-assembled microspheres with high stability for efficient solar-driven photocatalytic hydrogen evolution. *Inorg. Chem. Front.* **2023**, *10*, 1153−1163, DOI: 10.1039/D2QI02596E.
(23) Ivanovskaya, M.; Chernyakova, K.; Ovodok, E.; Poznyak, S.; Kotsikau, D.; Micusik, M. Synthesis and structural features of black TiO_2 nanotubes after annealing in hydrogen. *Mater. Chem. Phys.* **2023**, *297*, No. 127416.
(24) Liu, S.; Bao, L.; Jia, Q.; Qiao, X.; Wang, D. Controllable preparation of black titanium dioxide and its wave-absorbing properties. *Appl. Phys. A* **2023**, *129*, 119.
(25) Rajaraman, T. S.; Parikh, S. P.; Gandhi, V. G. Black TiO2: A review of its properties and conflicting trends. *Chem. Eng. J.* **2020**, *389*, No. 123918.
(26) Vijayarangamuthu, K.; Youn, J.-S.; Park, C.-M.; Jeon, K.-J. Facile synthesis of core−shell-structured rutile TiO2 with enhanced photocatalytic properties. *Catal. Today* **2018**, *347*, 18−22.
(27) Sun, W.; Guo, R.; Shi, C.; Li, X.; Wu, J.; Tian, H.; Li, H.; He, J.; Yang, Z.; Li, J.; Sun, S. Preparation and Photocatalytic Properties of CQDs-Modified 26-Facet Cu/Cu2O Composites. *Catal. Lett.* **2023**, DOI: 10.1007/s10562-023-04344-9.
(28) Cristino, A. F.; Matias, I. A. S.; Bastos, D. E. N.; Galhano dos Santos, R.; Ribeiro, A. P. C.; Martins, L. M. Glycerol Role in Nano Oxides Synthesis and Catalysis. *Catalysts* **2020**, *10*, 1406.
(29) Ishida, H.; Bünzli, J. C.; Beeby, A. Guidelines for measurement of luminescence spectra and quantum yields of inorganic and organometallic compounds in solution and solid state (IUPAC Technical Report). *Pure Appl. Chem.* **2016**, *88*, 701−711.
(30) Zhang, J.; Sun, L.; Yin, J.; Su, H.; Liao, C.; Yan, C. Control of ZnO morphology via a simple solution route. *Chem. Mater.* **2002**, *14*, 4172−4177.
(31) Marimuthu, S.; Rahuman, A. A.; Jayaseelan, C.; Kirthi, A. V.; Santhoshkumar, T.; Velayutham, K.; Bagavan, A.; Kamaraj, C.; Elango, G.; Iyappan, M.; Siva, C.; et al. Acaricidal activity of synthesized titanium dioxide nanoparticles using Calotropis gigantea against Rhipicephalus microplus and Haemaphysalis bispinosa. *Asian Pac. J. Trop. Med.* **2013**, *6*, 682−688.
(32) Sana, S. S.; Vadde, R.; Kumar, R.; Arla, S. K.; Somala, A. R.; Rao, K. K.; Zhijun, Z.; Boya, V. K.; Mondal, K.; Mamidi, N. Eco-friendly and facile production of antibacterial zinc oxide nanoparticles from Grewia flavescens (G. flavescens) leaf extract for biomedical applications. *J. Drug Delivery Sci. Technol.* **2023**, *80*, No. 104186.
(33) Srinivasan, M.; Venkatesan, M.; Arumugam, V.; Natesan, G.; Saravanan, N.; Murugesan, S.; Ramachandran, S.; Ayyasamy, R.; Pugazhendhi, A. Green synthesis and characterization of titanium dioxide nanoparticles (TiO_2 NPs) using Sesbania grandiflora and evaluation of toxicity in zebrafish embryos. *Process Biochem.* **2019**, *80*, 197−202.
(34) Rahman, S.; Nawaz, R.; Khan, J. A.; Ullah, H.; Irfan, M.; Glowacz, A.; Lyp-Wronska, K.; Wzorek, L.; Asif Khan, M. K.; Jalalah, M.; Alsaiari, M. A.; Almawgani, A. H. Synthesis and Characterization of Carbon and Carbon-Nitrogen Doped Black TiO_2 Nanomaterials and Their Application in Sonophotocatalytic Remediation of Treated Agro-Industrial Wastewater. *Materials* **2021**, *14*, 6175.
(35) Nawaz, R.; Kait, C. F.; Chia, H. Y.; Isa, M. H.; Huei, L. W.; Sahrin, N. T. Synthesis of Black-TiO_2 and manganese-doped TiO_2 nanoparticles and their comparative performance evaluation for photocatalytic removal of phenolic compounds from agro-industrial effluent. *J. Nanopart. Res.* **2021**, *23*, 263.
(36) Vidya, C.; Manjunatha, C.; Chandraprabha, M. N.; Rajshekar, M.; Mal, A. R. Hazard free green synthesis of ZnO nano-photocatalyst using Artocarpus Heterophyllus leaf extract for the degradation of Congo red dye in water treatment applications. *J. Environ. Chem. Eng.* **2017**, *5*, 3172−3180.
(37) Nawaz, R.; Kait, C. F.; Chia, H. Y.; Isa, M. H.; Huei, L. W.; Sahrin, N. T.; Khan, N. Manipulation of the Ti^{3+}/Ti^{4+} ratio in colored titanium dioxide and its role in photocatalytic degradation of environmental pollutants. *Surf. Interfaces* **2022**, *32*, No. 102146.
(38) Gonçalves, R. A.; Toledo, R. P.; Joshi, N.; Berengue, O. M. Green Synthesis and Applications of ZnO and TiO_2 Nanostructures. *Molecules* **2021**, *26*, 2236.
(39) Gomathi, R.; Suhana, H. Green synthesis, characterization and antimicrobial activity of zinc oxide nanoparticles using Artemisia pallens plant extract. *Inorg. Nano-Met. Chem.* **2021**, *51*, 1663−1672.
(40) Kumar, P. M.; Badrinarayanan, S.; Sastry, M. Nanocrystalline TiO_2 studied by optical, FTIR and X-ray photoelectron spectroscopy:

https://doi.org/10.1021/acsomega.3c04229
ACS Omega 2023, 8, 36076−36087

correlation to presence of surface states. *Thin Solid Films* **2000**, *358*, 122−130.
(41) Ren, T. Z.; Yuan, Z. Y.; Su, B. L. Surfactant-assisted preparation of hollow microspheres of mesoporous TiO_2. *Chem. Phys. Lett.* **2003**, *374*, 170−175.
(42) Eom, J. Y.; Lim, S. J.; Lee, S. M.; Ryu, W. H.; Kwon, H. S. Black titanium oxide nanoarray electrodes for high rate Li-ion micro-batteries. *J. Mater. Chem. A* **2015**, *3*, 11183−11188.
(43) Karidas, S.; Veena, B. K.; Pujari, N.; Krishna, P.; Chunduru, V. Photodegradation of methylene blue (MB) using cerium-doped zinc oxide nanoparticles. *Sādhanā* **2020**, *45*, 128.
(44) Turkten, N.; Bekbolet, M. Photocatalytic performance of titanium dioxide and zinc oxide binary system on degradation of humic matter. *J. Photochem. Photobiol. A* **2020**, *401*, No. 112748.
(45) Payra, S.; Challagulla, S.; Bobde, Y.; Chakraborty, C.; Ghosh, B.; Roy, S. Probing the photo- and electro-catalytic degradation mechanism of methylene blue dye over ZIF-derived ZnO. *J. Hazard. Mater.* **2019**, *373*, 377−388.
(46) Sarkar, S.; Makhal, A.; Baruah, S.; Mahmood, M. A.; Dutta, J.; Pal, S. K. Nanoparticle-sensitized photodegradation of bilirubin and potential therapeutic application. *J. Phys, Chem. C* **2012**, *116*, 9608−9615.
(47) Tho, N. T.; Thi, C. M.; Van Hieu, L.; Van Viet, P. Visible-light-driven photocatalysis for methylene blue degradation and hydrogen evolution reaction: a case of black TiO_2 nanotube arrays. *J. Aust. Ceram. Soc.* **2020**, *56*, 849−857.
(48) Zaid, E. H. A.; Sin, J. C.; Lam, S. M.; Mohamed, A. R. Fabrication of La, Ce co-doped ZnO nanorods for improving photodegradation of methylene blue. *J. Rare Earths* **2023**, DOI: 10.1016/j.jre.2023.02.001.
(49) Jing, L.; Xin, B.; Yuan, F.; Xue, L.; Wang, B.; Fu, H. Effects of surface oxygen vacancies on photophysical and photochemical processes of Zn-doped TiO_2 nanoparticles and their relationships. *J. Phys. Chem. B* **2006**, *110*, 17860−17865.
(50) Pawar, M.; Nimbalkar, V. Synthesis and phenol degradation activity of Zn and Cr doped TiO_2 Nanoparticles. *Res. J. Chem. Sci.* **2012**, *2*, 32−37.
(51) Naik, B.; Parida, K. Solar Light Active Photodegradation of Phenol over a Fe_xTi_{1-x} O_{2-y} N_y Nanophotocatalyst. *Ind. Eng. Chem. Res.* **2010**, *49*, 8339−8346.
(52) Reza, K. M.; Kurny, A. A. W.; F Gulshan, F. Parameters affecting the photocatalytic degradation of dyes using TiO_2: a review. *Appl. Water Sci.* **2017**, *7*, 1569−1578.
(53) Lin, J.; Luo, Z.; Liu, J.; Li, P. Photocatalytic degradation of methylene blue in aqueous solution by using ZnO-SnO_2 nano-composites. *Mater. Sci. Semicond. Process.* **2018**, *87*, 24−31.
(54) Sobczyński, A.; Duczmal, L.; Zmudziński, W. Phenol destruction by photocatalysis on TiO_2: an attempt to solve the reaction mechanism. *J. Mol. Catal. A* **2004**, *213*, 225−230.
(55) Jay, L.; Chirwa, E. Pathway Analysis of Phenol Degradation by UV/TiO_2 Photocatalysis Utilising the C-13 Isotopic Labelling Technique. *Chem. Eng. Transac.* **2018**, *70*, 181−186 DOI: 10.3303/CET1870031.
(56) Zulfiqar, M.; Samsudin, M. M. F.; Sufian, S. Modelling and optimization of photocatalytic degradation of phenol via TiO_2 nanoparticles: An insight into response surface methodology and artificial neural network. *J. Photochem. Photobiol. A* **2019**, *384*, No. 112039.
(57) Feng, C.; Chen, Z.; Jing, J.; Hou, J. The photocatalytic phenol degradation mechanism of Ag-modified ZnO nanorods. *J. Mater. Chem. C* **2020**, *8*, 3000−3009.

https://doi.org/10.1021/acsomega.3c04229
ACS Omega 2023, 8, 36076−36087